Analysis of array forming using the Blackfoot high-resolution 3-C data

Brian H. Hoffe, Darren S. Foltinek, Henry C. Bland, Gary F. Margrave and Peter M. Manning

ABSTRACT

During November 1997 the CREWES Project at the University of Calgary recorded a 3C-2D seismic survey at the Blackfoot field east of Calgary. This survey consisted of recording dynamite shots into a combination of conventional 20 m and high-resolution 2 m receiver intervals. We used this high-resolution data to examine two alternative approaches to array design by simulating 3-C receiver arrays via convolution in the *t-x* domain. The effectiveness of each approach was then evaluated by analysing the response in both the *t-x* and *f-k* domains. The post-stack effect was also compared by analysing the *f-x* response of both the final P-P and P-S structure stacks produced using these two array design philosophies.

The pre-stack analysis showed that these two approaches were effective in suppressing coherent noise on both the vertical and radial data and performed reasonable well as anti-alias filters. The post-stack analysis revealed that for both the P-P and P-S data neither of the two design approaches improved the quality of the final seismic image over that obtained from non-arrayed data. For the P-P data there was no discernible difference between the final stacked sections, while for the P-S data there was a noticeable deterioration in image quality from the application of arrays. Thus we conclude that, for the Blackfoot area, given the source configuration used, field implementation of 3-C arrays are unnecessary for P-P data acquisition and are certainly detrimental to the recording of P-S data.

INTRODUCTION

The traditional method of attenuating coherent noise in the seismic field recording has been through the use of source and receiver arrays (Newman and Mahoney, 1973). The array sums the signals from a pattern of sources or receivers in order to attenuate source-generated and off-line coherent noise while attempting to preserve as much of the seismic signal as possible (Stone, 1994). The underlying principal of the receiver array lies in the observation that desired reflection events propagate across the array with a much higher *apparent* velocity (apparent velocity is $v/\sin\theta$ where v is wave speed and θ is emergence angle) than that of the undesired surface waves such as air blast and ground roll. Thus, for any given frequency, the noise horizontal wavelength, λ_x, will be shorter, or equivalently, the noise wavenumber, $k_x = 1/\lambda_x$, will be greater. As Onkiehong and Askin (1988) point out, this is a key observation as it indicates that for any desired frequency, signal is separable from noise by application of an appropriate wavenumber filter. Such a filter is immediately provided by the grouping of adjacent geophones into arrays.

However, Onkiehong and Askin (1988) also point out, the use of the receiver array as a wavenumber filter is not without compromise. The separation of signal and noise is frequency dependent. Thus for a given array design, placing a rejection notch at a specific noise wavenumber may also lead to significant attenuation of the reflected signal depending on the actual apparent velocity of the reflected wavefront at the array location. A far better signal/noise separator is an *f-k* fan filter which an array cannot inherently achieve. Newman and Mahoney (1973) pointed to other problems inherent with the use of field arrays. They demonstrated that although complex (i.e. weighted) arrays could be designed with virtually any desired response in the wavenumber domain, these arrays could not be practically deployed with the same precision that was used in their design. The actual array response achieved is compromised by a number of factors. These include inaccuracies in positioning of the individual array elements, variations in ground coupling and the effect of local heterogeneities in the array environment.

There appears to be two schools of thought regarding the field deployment of arrays (refer to Figure 3). The first school, which is probably the more widely accepted, advocates using an array length, L, equal to twice the group interval, ΔG (i.e. $L = 2\Delta G$). We refer to this as the "noise aggressive" approach. Using this approach, the primary rejection notch of the array response in the *f-k* domain (i.e. $\pm 1/L$) will equal the spatial nyquist, $|k_n| = 1/2\Delta G$, defined by the group interval (i.e. $1/L = 1/2\Delta G$). Thus aliased energy (i.e. signal and noise) will be significantly attenuated due to the fact that it will all lie within the array reject band. However, depending on whether there is significant reflected energy as k_n is approached, this method may also unfortunately attenuate signal. The second school advocates using an array length equal to the group interval (i.e. $L = \Delta G$; Onkiehong and Huizer, 1987; Onkiehong and Askin, 1988). We refer to this as the "signal preferred" approach. In this approach, the primary rejection notch of the of the array response in the *f-k* domain will be twice the spatial nyquist (i.e. $1/L = 1/\Delta G$). This ensures that unaliased energy (i.e. signal and noise) will be mostly preserved because it will all lie within the array pass band. However, this approach may lead to strong aliasing of both noise *and* signal since the aliased energy beyond the spatial nyquist will not be strongly rejected.

During November 1 – 2, 1997 the CREWES Project, with assistance from Boyd PetroSearch Consultants Ltd. and PanCanadian Petroleum Ltd., recorded a unique, high-resolution 3C-2D seismic survey at the Blackfoot oil and gas field. This survey involved the acquisition of a 3 km 3C-2D reflection profile which consisted of a combination of conventional and high-resolution receiver intervals (Hoffe et al., 1998). A schematic diagram of the survey layout is presented in Figure 1. The source interval employed for the entire profile was 20 m. However, the receiver interval changed from 20 m to 2 m in the central km of the profile. To examine the effect of these two approaches to array design, we used this high-resolution data to simulate 3-C receiver arrays with: a) array length, L, equal to twice the group interval ($L = 2\Delta G; \Delta G = 20\,\text{m}$), and b) array length, L, equal to the group interval ($L = \Delta G$). This was done by convolving a space series defining each of the two array designs with both the vertical and radial source gathers in the *t-x* domain and then re-sampling

Contents

to the group interval. The effectiveness of each array applied was then evaluated by analysing its response in both the *t-x* and *f-k* domains. The post-stack effect was also compared by analysing the *f-x* response of both the P-P and P-S structure stacks produced from the array formed shot gathers.

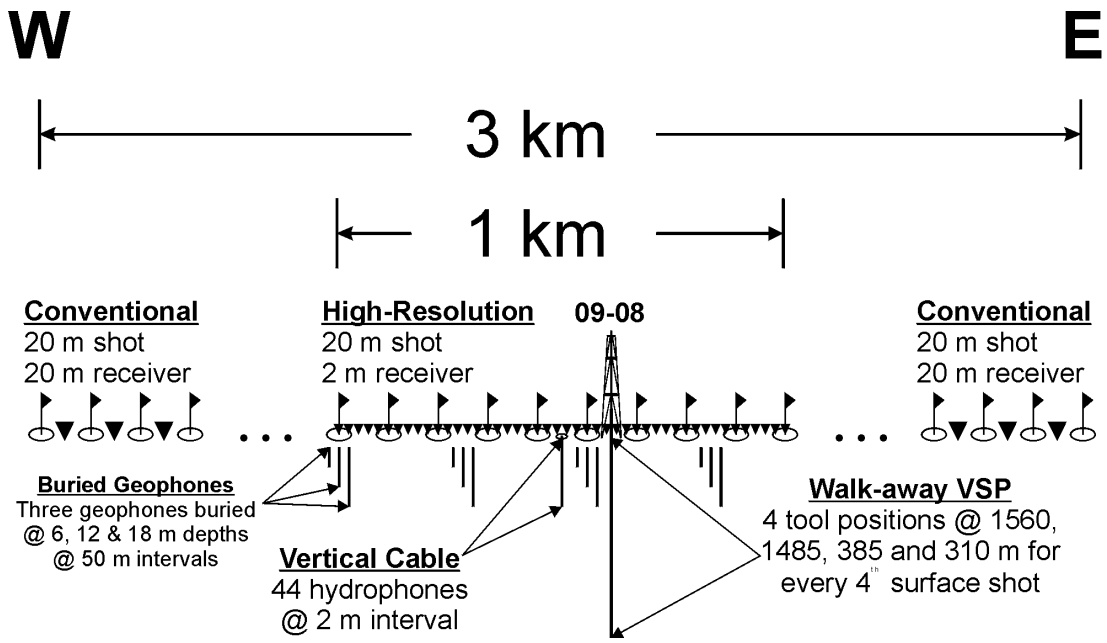

Figure 1. Schematic diagram (not to scale) illustrating the layout of the Blackfoot 3C-2D high-resolution seismic survey (after Hoffe et al., 1998).

METHODOLOGY

The Blackfoot high-resolution 3-C data was processed commercially by Matrix Geoservices Ltd. Upon completion of processing, Matrix kindly provided us with the ProMAX ™ archive containing all data and processing flows which was subsequently loaded for use here at the CREWES Project. This gave us a much greater flexibility in the in-house manipulation and extraction of the data required for the array forming and allowed us to copy and modify the previous processing flows required for our post-stack analysis.

1) Pre-Stack Array Forming

All of the pre-stack array forming and analysis was done via MATLAB™. The input into MATLAB™ (via SEG-Y output from ProMAX ™) consisted of both a vertical and radial source gather for a common source point containing only the receivers encompassing the high-resolution portion of the survey. An "end-on" source-receiver configuration was chosen for the analysis with the source being located only 10 m from the first live receiver of the high-resolution spread. Choosing this configuration essentially yields a "noise spread" which is so often used in the analysis of source-generated coherent noise prevalent on the seismic field recording.

Contents

The response of a linear array can be analysed by considering the idealised response of a sequence of unit spikes (Figure 2). Since the array is purely a function of *x*, its response, when Fourier transformed into the *f-k* domain, is purely a function of wavenumber, *k*. Thus for a *N*-element array with an inter-array spacing of Δx and length L ($L = N\Delta x$), its pass band is defined by $k = \pm 1/L$ and reject band defined by $|k| > 1/L$ with notches occurring at $k = \pm n/L$ where $n = 1,2,\ldots N-1$.

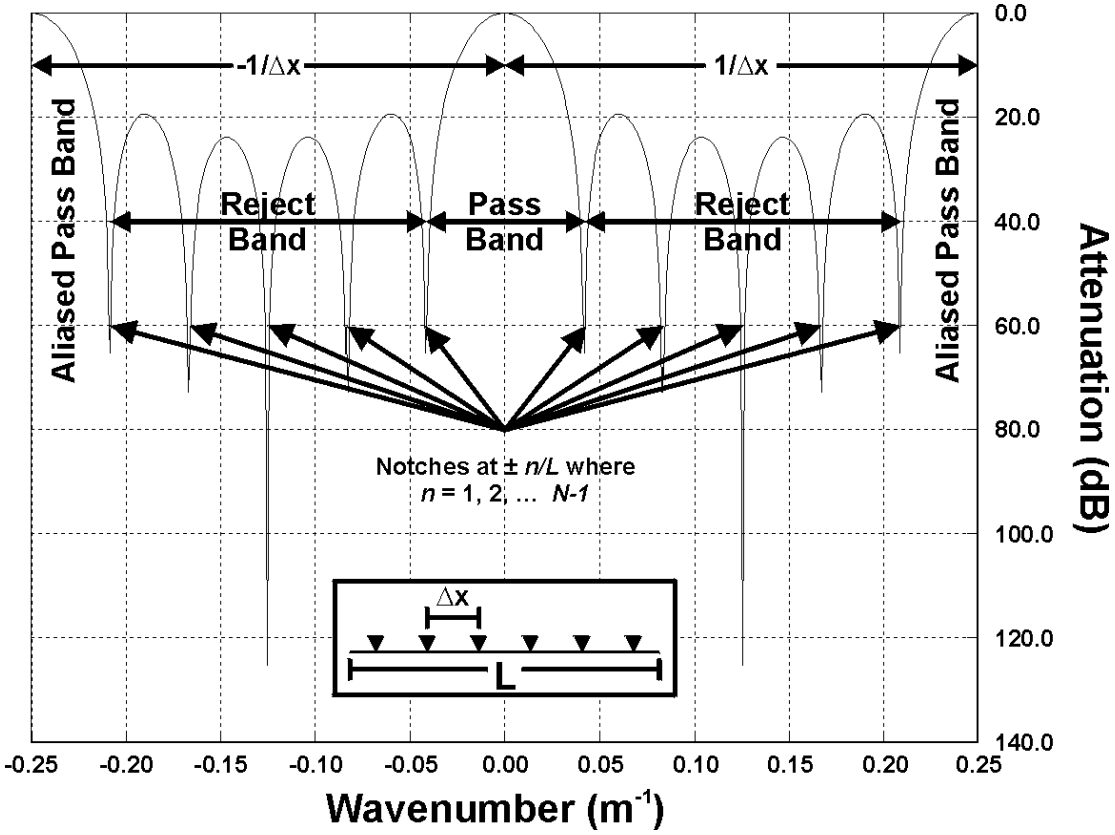

Figure 2. *f-k* domain response of a linear array. The linear array (see inset) is defined in terms of its length, L, and the inter-array spacing, Δx. In the *f-k* domain the pass band is defined by $k = \pm 1/L$, the reject band by $|k| > 1/L$ and the rejection notches occur at $k = \pm n/L$ where $n = 1,2,\ldots N-1$.

Thus array forming in the *t-x* domain can be accomplished by simply convolving the source gathers with a "space" series consisting of a sequence of ones and zeros at an inferred spatial sampling interval, Δx (i.e. 2 m - the receiver spacing of the high-resolution data itself). For instance, to define a five element array with an inter-array spacing of 6 m (i.e. N=5, Δx=6 & L=30), the space series would be defined as (1, 0, 0, 1, 0, 0, 1, 0, 0, 1, 0, 0, 1). This series would then be convolved with both the vertical and radial source gather. After convolution, the array-formed shot gathers, still at their original 2 m trace spacing, were transformed into the *f-k* domain to analyse the effect of the array forming operation on the *f-k* spectra.

Contents

The next step was to re-sample the array-formed source gathers from their original receiver spacing of 2 m to the more conventional group spacing of 20 m as was used in the 1st and 3rd kilometres of the 3C-2D reflection profile (see Figure 1). An important consequence of this re-sampling process is the dramatic change in the spatial nyquist and consequent aliasing. The spatial nyquist, defined as $k_n = \pm 1/2\Delta x$, changes from 0.25 m^{-1} for the 2 m spacing to 0.025 m^{-1} for the 20 m spacing – a factor of 10 in the difference. As a result, all energy present in the array formed *f-k* spectrum with wavenumbers of $|k| > k_{new}$, where k_{new} is the new spatial nyquist upon re-sampling (i.e. $|k_{new}| = 1/2\Delta G$), will be subsequently aliased or folded back at $\pm k_{new}$ into the *f-k* spectrum of the re-sampled source gathers.

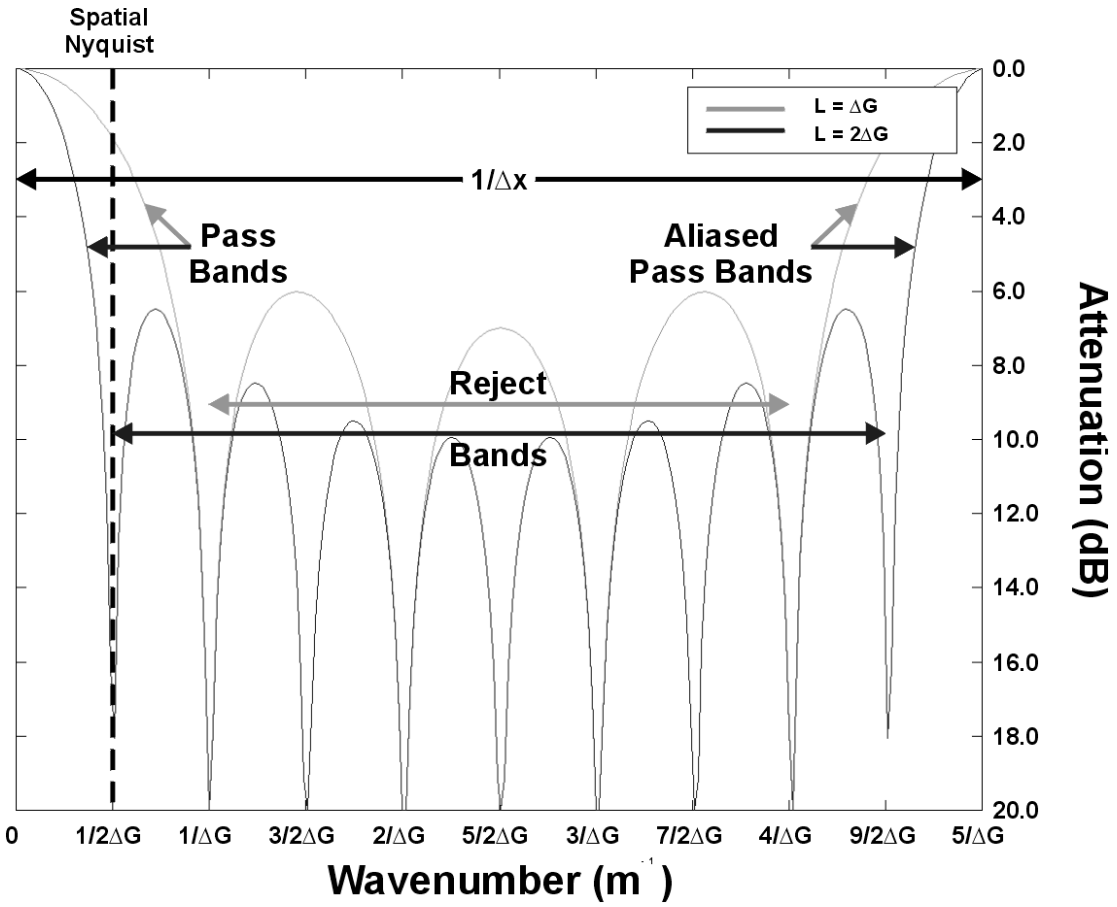

Figure 3. Comparison of the *f-k* responses for arrays $L = 2\Delta G$ and $L = \Delta G$. Note that for the array where $L = 2\Delta G$ the primary rejection notch falls at $1/L = 1/2\Delta G$, the new spatial nyquist determined by the group interval. For the array where $L = \Delta G$, the rejection notch falls at $1/L = 1/\Delta G$ or twice the new spatial nyquist.

Thus an important consideration in analysing the *f-k* spectrum of the array formed and re-sampled source gathers is examining the effectiveness of the anti-aliasing properties of the array itself. That is to say, where is the primary rejection notch of the array response positioned with respect to the new spatial nyquist? The answer to this question leads us back to the two array designs approaches previously discussed: (a)

Contents

the "noise aggressive" approach where $L = 2\Delta G$ or $1/L = 1/2\Delta G$ and, (b) the "signal preferred" approach where $L = \Delta G$ or $1/L = 1/\Delta G$. Figure 3 illustrates the *f-k* domain differences between these two approaches. The "noise aggressive" approach will significantly attenuate aliased energy (i.e. signal and noise) but, depending on whether there is significant reflected energy as k_{new} is approached, may also unfortunately attenuate signal. The "signal preferred" approach ensures that unaliased energy (i.e. signal and noise) will be mostly preserved but may lead to strong aliasing since k_{new} and the aliased energy (i.e. signal and noise) beyond it will not all be strongly rejected.

Given the geometry of the high-resolution data set, any number of array configurations could have been simulated for this particular study but we chose only to examine the two cases described above. The two array configurations selected were chosen as to be economically feasible in terms of their field deployment. The key parameters defining the two arrays used are itemised in Table 1 below.

Table 1. Parameters for the arrays used in this study; N = number of elements, Δx = inter-array spacing, L = array length, $1/\Delta x$ = location of the aliased pass band and $1/L$ = location of primary rejection notch.

N	Δx (m)	L (m)	$1/\Delta x$ (m^{-1})	$1/L$ (m^{-1})
10	4	40	0.25	0.025
5	4	20	0.25	0.050

2) Post-Stack Array Comparisons

In order to produce the various P-P and P-S arrayed stacks to be used for post-stack comparisons, ProMAX ™ was used as it allowed us to copy and modify the processing flows previously used by Matrix Geoservices. For array implementation in ProMAX™, a custom program module was written which allowed for each of the arrays prescribed in Table 1 (and, due to the module's flexibility, any others the user wished to define) to be applied to the high-resolution shot gathers. This custom module, upon completion of the array forming operation, also spatially re-sampled the shot-ordered data to the 20 m group interval as was done in the pre-stack array forming.

The processing flows used to produce the P-P and P-S arrayed stacks are listed in Tables 2 and 3 respectively. Both P-P and P-S stacks at the re-sampled 20 m group interval (i.e. 10 m bin interval) were produced for each array configuration listed in Table 1 plus a non-arrayed version of both P-P and P-S. These stacks were then input into MATLAB™ (via SEG-Y output from ProMAX ™) for *f-x* analysis (Margrave, 1995).

Final unmigrated P-P and P-S stacks produced from the arrayed and non-arrayed shot gathers (see data processing) were analysed for changes in event continuity in the *f-x* domain. *f-x* spectra were calculated over the stacked sections, using a time

window approximately centred at the glauconitic channel, which is the exploration target in the Blackfoot area. For the P-P data, the channel lies at approximately 1100 ms, and the analysis window used was 700 – 1200 ms. For the P-S data, the channel lies at approximately 1600 ms, and the window used was 1200 – 1700 ms.

Table 2. Processing flow used to produce the arrayed P-P stacks.

1. Geometry, Trace Kills & Reversals
2. True Amplitude Recovery
3. Array Forming
4. Surface-Consistent Deconvolution + TVSW
5. Refraction Statics + Surface Consistent Statics
6. CDP Trim Statics
7. NMO
8. Trace Muting
9. TV Scaling
10. CDP Stack

Table 3. Processing flow used to produce the arrayed P-S stacks.

1. Geometry, Trace Kills & Reversals
2. True Amplitude Recovery
3. Array Forming
4. Surface-Consistent Deconvolution + TVSW
5. Vertical Component Statics + Residual Receiver Statics
6. Surface Consistent Statics
7. ACP Trim Statics
8. Converted Wave NMO
9. Trace Muting
10. TV Scaling
11. CCP Stack

Two different numerical comparison methods were utilised to help quantify the differences between the *f-x* spectra of the final stacks. The first method computed an average amplitude spectrum over a 50 trace window centred on the stack. To equalise power in each of the spectra, they were decibel scaled relative to their respective RMS amplitude of the high frequency noise band. For the P-P data, this noise band ranged from 170 to 250 Hz. For the P-S data, the noise band went from 100 to 150 Hz. This was done in an attempt to minimise any power differences between each of the final stacks. The averaged spectra were then subtracted to emphasise differences.

The second numerical comparison technique used was a semblance measure on each of the *f-x* spectra. The spectral semblance, S, is defined as:

$$S = \frac{\left| \sum_{x=1}^{N} C_x \right|}{\sum_{x=1}^{N} |C_x|} \qquad (1)$$

where C_x is the complex spectrum of each trace. The summation is performed over a range of traces (i.e. with respect to x) which yields the semblance as a function of frequency. For these semblance computations, the *t-x* windows previously described for the *f-x* average amplitude analysis were again used. These semblance curves were also differenced.

Contents

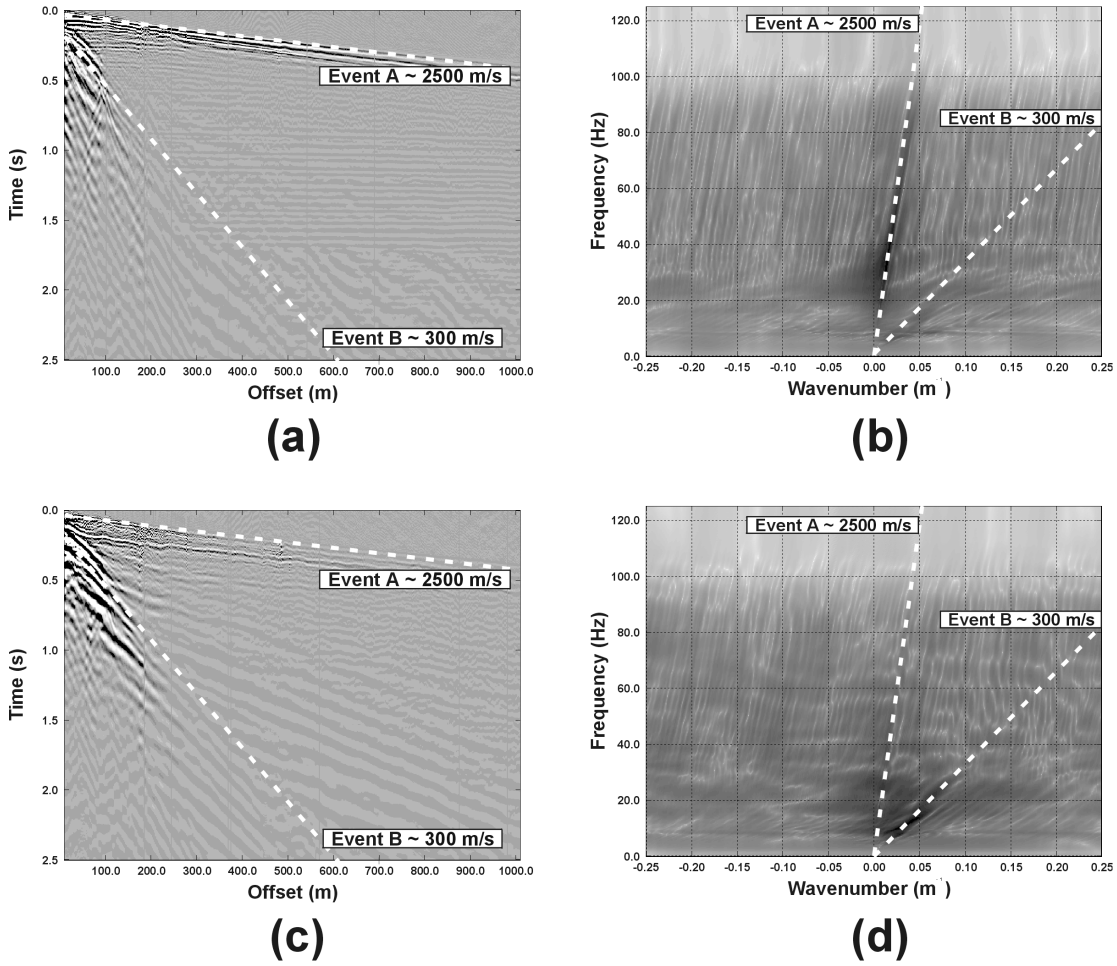

Figure 4. (a) *t-x* display of the "raw" vertical source gather used for the pre-stack analysis and (b) its corresponding *f-k* amplitude spectrum; (c) *t-x* display of the "raw" radial source gather used for the pre-stack analysis and (d) its corresponding *f-k* amplitude spectrum. *f-k* spectra are plotted in a decibel grey-scale with black representing the strongest power.

RESULTS

1) Pre-Stack Array Forming

Figure 4 shows *t-x* displays of the vertical and radial source gathers that were used for analysis and their corresponding *f-k* spectra. The source gathers have no amplitude recovery or gain applied and are presented in their raw form. The vertical source gather and its *f-k* spectrum (Figure 4a and 4b respectively) shows that the dominant energy lies in the first break or head wave labelled "Event A". However, there also appears to be significant energy in what appears to be air blast, labelled "Event B", given its approximate apparent velocity of 300 m/s. Also, the reflected energy is clearly visible on the vertical source gather as a series of essentially flat-lying events (i.e. apparent velocity ~ ∞). In contrast, the radial source gather and its *f-k* spectrum (Figure 4c and 4d respectively) indicates that a majority of its energy lies in the air blast with secondary energy contained within the first break. In addition to these two events, the *t-x* display of the radial source gather also shows a series of linear dipping

Contents

events with an apparent velocity of ~ 600 – 700 m/s which is assumed to be ground roll.

Figure 5 again displays the *t-x* plot for the "raw" vertical source gather and its corresponding *f-k* spectrum (a and b) but also includes the *t-x* vertical arrayed gathers and their *f-k* spectra for arrays $L = 40$ (c and d) and $L = 20$ (e and f) for comparison. Starting first with the *t-x* plots, there is a noticeable improvement in the lateral continuity of the reflectors on the arrayed gathers in the range of 250 – 400 m offset between 1.5 – 1.6 s as compared to the non-arrayed gather. This improvement in reflector continuity is largely due to the suppression of the air blast noise train (Event B; 0.2 s, 0.0 m offset $\rightarrow$ 2.5 s, 600 m offset) due to the application of the arrays. The *f-k* spectra of the arrayed gathers have their respective array response curves (in dB scale) overlaid to show the location of the pass and reject bands with respect to the dominant energy present in the spectra. It is important to note that, as expected, the primary rejection notch of the 20 m array (± 0.050 m^{-1}) is twice that of the 40 m array (± 0.025 m^{-1}). Consequently, the width of pass band for the 20 m array is twice that of the 40 m array. The width of the reject band, however, for the 20 m array is comparable to the 40 m array (0.15 m^{-1} vs. 0.20 m^{-1}) but the peak attenuation over this reject band is somewhat greater for the 40 m array (20 dB vs. 14 dB).

Similarly, Figure 6 displays the *t-x* plot for the "raw" radial source gather and its corresponding *f-k* spectrum (a and b) as well as the *t-x* radial arrayed gathers and their *f-k* spectra for arrays $L = 40$ (c and d) and $L = 20$ (e and f) for comparison. The *t-x* plots for the arrayed source gathers again display significant attenuation of the air blast noise train as compared to the non-arrayed gather. The array response curves have again been overlaid on the *f-k* spectra and all the response characteristics and comparisons previously described for the vertical would also apply here for the radial. Also of note, the *f-k* spectra of the arrayed radial gathers show a considerable increase in relative energy in the vicinity of $k = 0$ compared to the *f-k* spectrum of the non-arrayed gather.

Figure 7 displays the *t-x* plot for the "raw" vertical source gather re-sampled to the 20 m group interval and its corresponding *f-k* spectrum (a and b) and the *t-x* re-sampled vertical arrayed gathers and their *f-k* spectra for arrays $L = 40$ (c and d) and $L = 20$ (e and f) for comparison. As with the original 2 m arrayed gathers, the *t-x* plots for the arrayed and re-sampled gathers also show the improvement in reflector continuity with the attenuation of the air blast. An important note about these *f-k* spectra is the change in the spatial nyquist from ± 0.25 m^{-1} for the original 2 m data to ± 0.025 m^{-1} for the re-sampled 20 m data. As a consequence, the re-sampled spectra represent only a very small segment of the original 2 m spectra or, in essence, a magnification, centred at $k = 0$ and all energy in the original spectra lying beyond the new spatial nyquist (i.e. ± 0.025 m^{-1}) will be folded-back or aliased. Thus the *f-k* spectra of the arrayed and re-sampled gathers should give some indication as to the effectiveness of each array as an anti-alias filter. As is evident for examination of Figure 7d and 7f, these *f-k* spectra reveal that there is considerably less energy being aliased or "wrapped" at the 50-55 Hz range as compared to the non-arrayed and re-sampled spectrum. Indeed the $L = 40$ array outperforms the $L = 20$ array as an anti-alias filter as its *f-k* spectrum (6d) shows less energy wrapping. This is expected as the

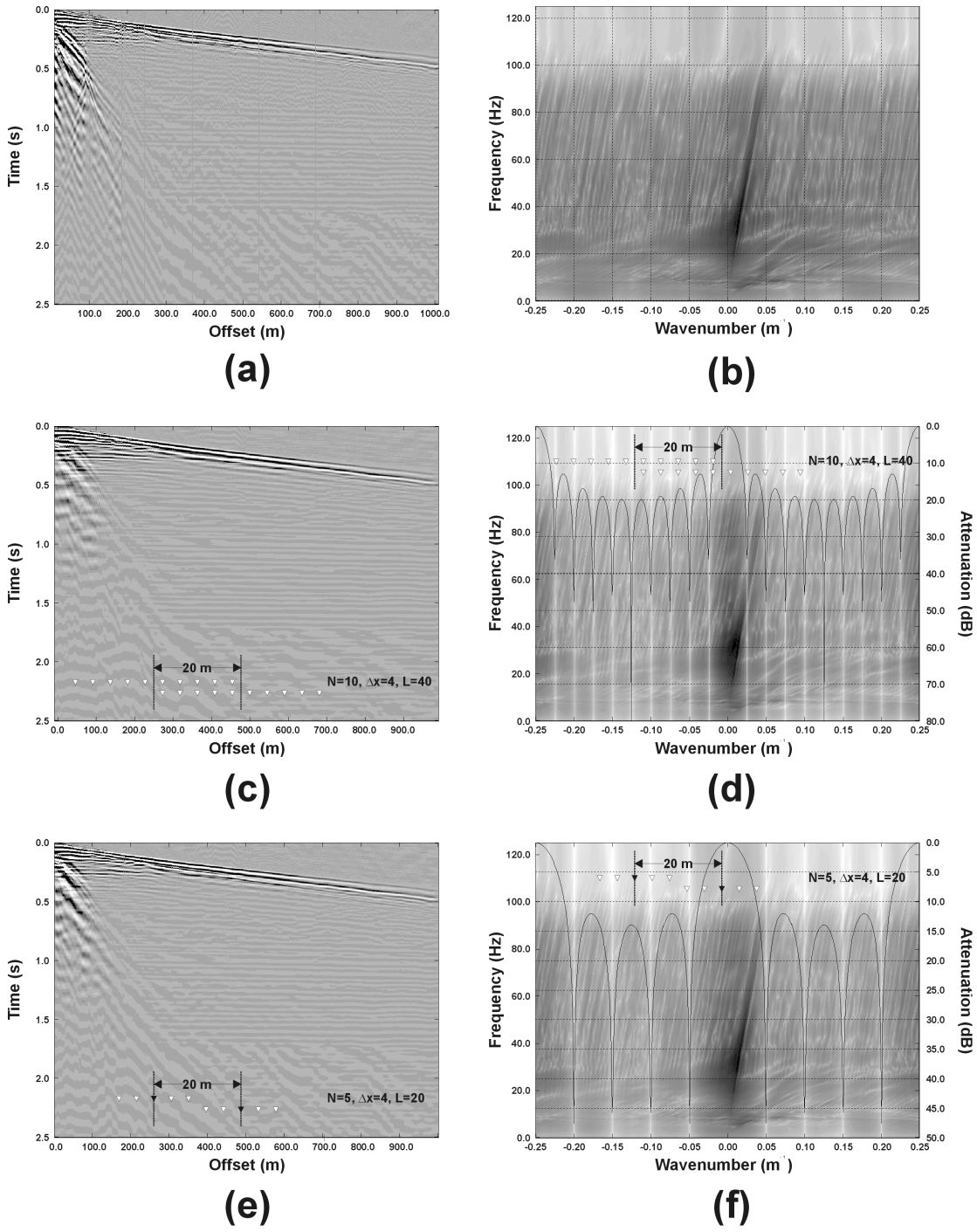

Figure 5. (a) *t-x* plot for the "raw" vertical source gather and (b) its corresponding *f-k* amplitude spectrum; (c) *t-x* vertical arrayed gather for the $L = 40$ array and (d) its corresponding *f-k* amplitude spectrum; (e) *t-x* vertical arrayed gather for the $L = 20$ array and (f) its corresponding *f-k* amplitude spectrum.

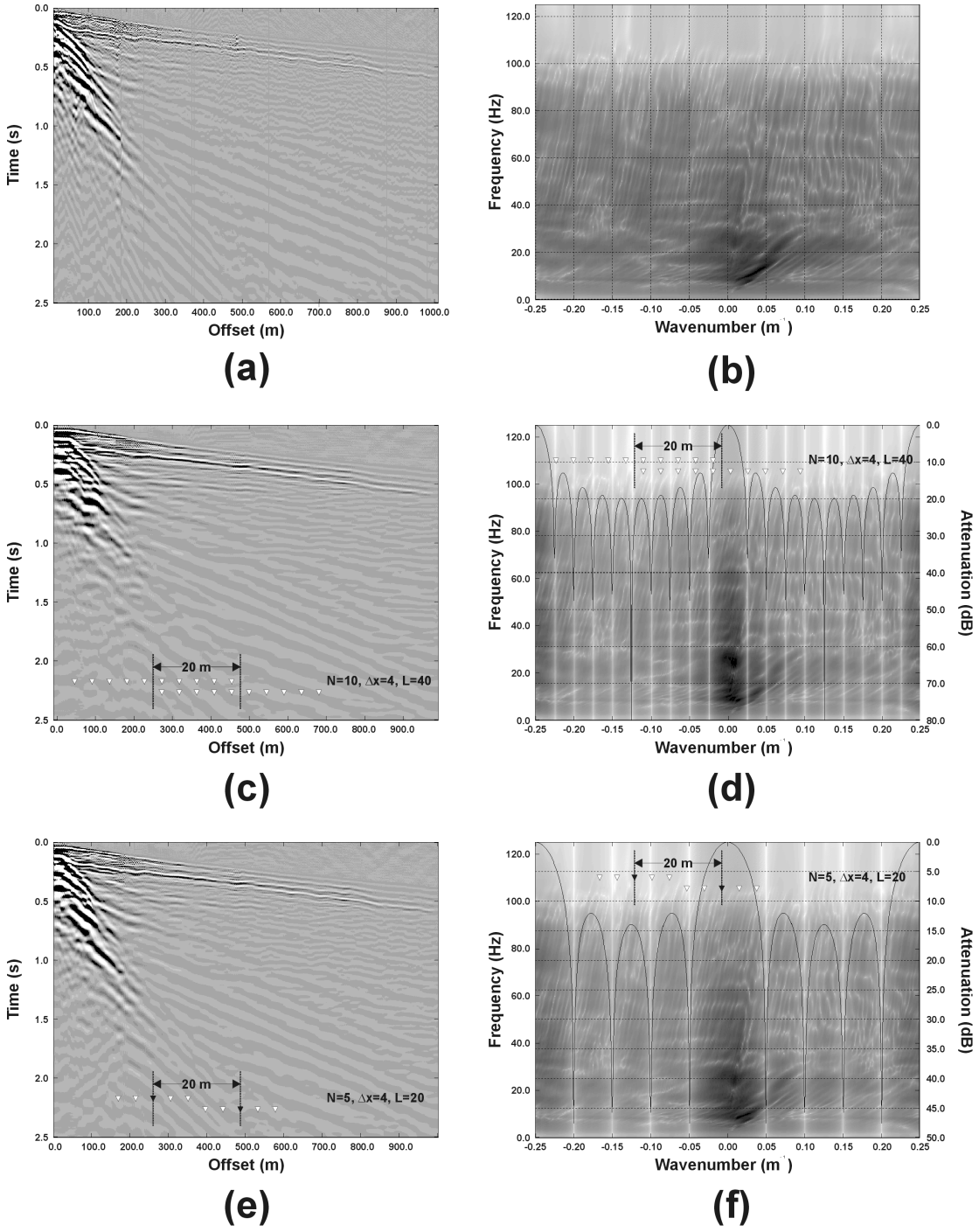

Figure 6. (a) *t-x* plot for the "raw" radial source gather and (b) its corresponding *f-k* amplitude spectrum; (c) *t-x* radial arrayed gather for the $L = 40$ array and (d) its corresponding *f-k* amplitude spectrum; (e) *t-x* radial arrayed gather for the $L = 20$ array and (f) its corresponding *f-k* amplitude spectrum.

Contents

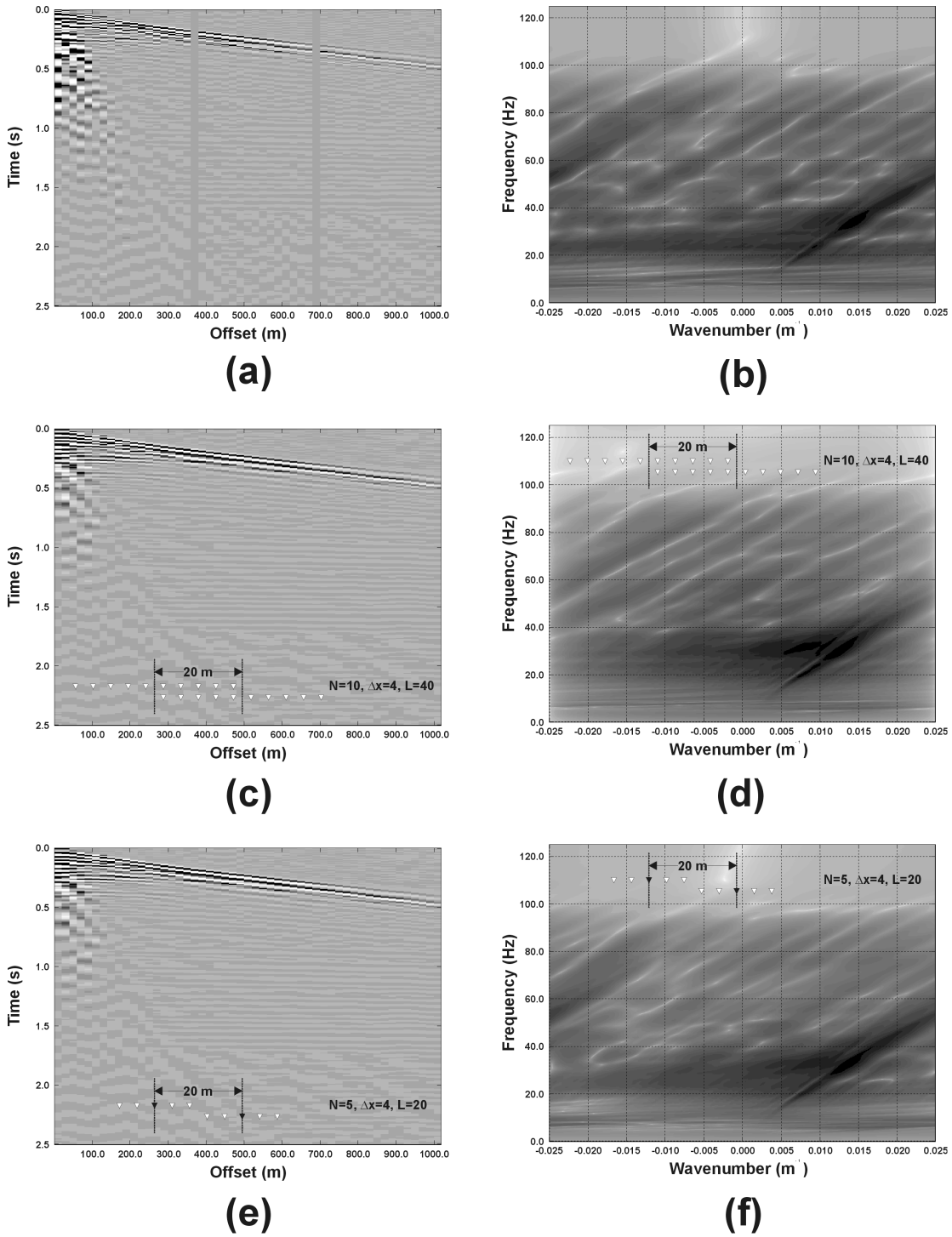

Figure 7. (a) *t-x* plot for the "raw" vertical source gather re-sampled to the 20 m group interval and (b) its corresponding *f-k* amplitude spectrum; (c) *t-x* re-sampled vertical arrayed gather for the $L = 40$ array and (d) its corresponding *f-k* amplitude spectrum; (e) *t-x* re-sampled vertical arrayed gather for the $L = 20$ array and (f) its corresponding *f-k* amplitude spectrum.

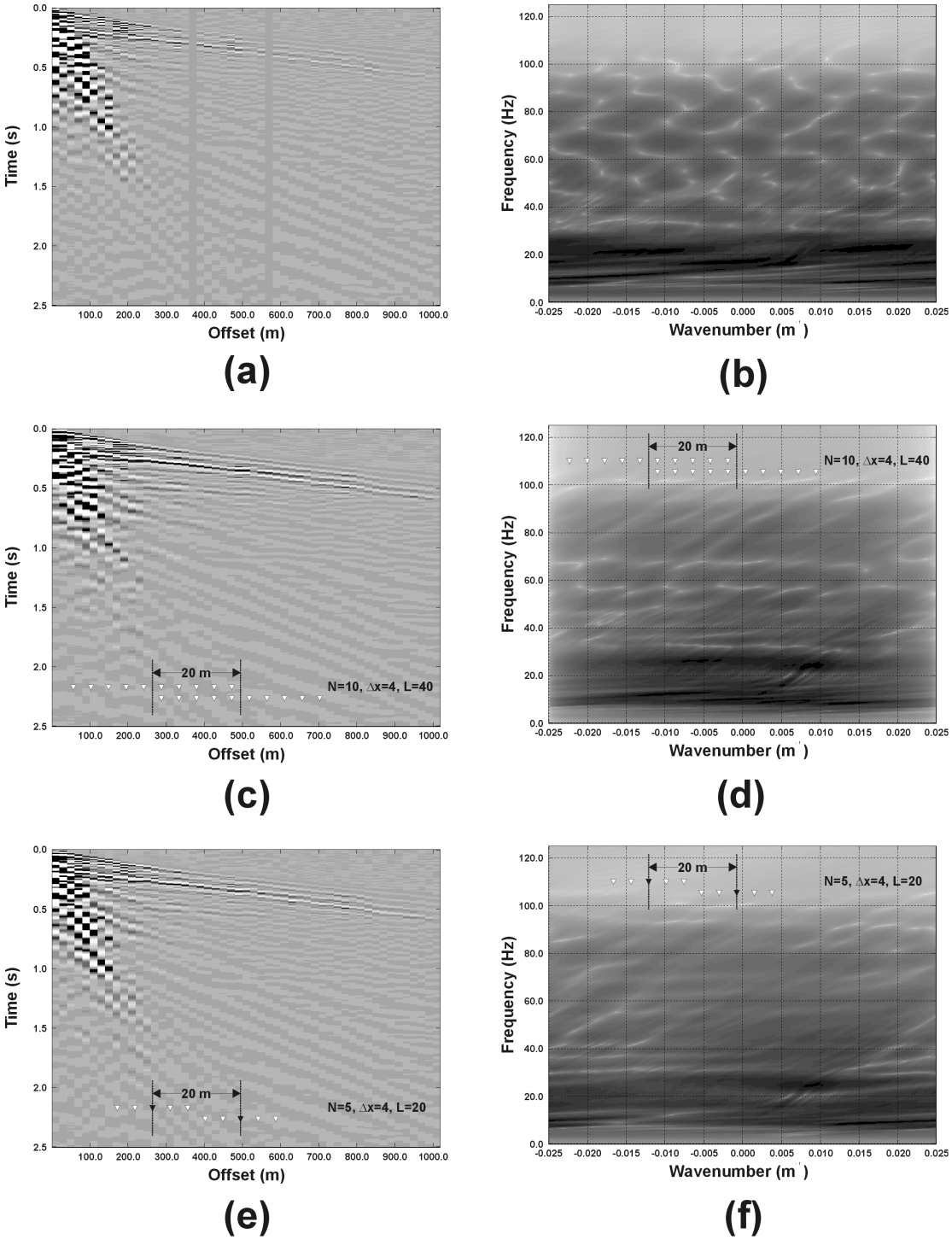

Figure 8. (a) *t-x* plot for the "raw" radial source gather re-sampled to the 20 m group interval and (b) its corresponding *f-k* amplitude spectrum; (c) *t-x* re-sampled radial arrayed gather for the $L = 40$ array and (d) its corresponding *f-k* amplitude spectrum; (e) *t-x* re-sampled radial arrayed gather for the $L = 20$ array and (f) its corresponding *f-k* amplitude spectrum.

Contents

primary rejection notch for the 40 m array lies exactly at the re-sampled spatial nyquist whereas the notch for the 20 m array lies at twice this new spatial nyquist (i.e. ± 0.05 m^{-1}). Thus all aliased energy for the 40 m array has been significantly attenuated since all falls within reject band prior to fold-back.

Figure 8 displays the *t-x* plot for the "raw" radial source gather re-sampled to the 20 m group interval and its corresponding *f-k* spectrum (a and b) and the *t-x* re-sampled radial arrayed gathers and their *f-k* spectra for arrays $L = 40$ (c and d) and $L = 20$ (e and f) for comparison. Again the *t-x* plots of the arrayed and re-sampled data show some attenuation of the air blast but apparently not as definitively as seen on the vertical data. This is probably due to the air blast dominating the energy recorded on the radial channel. The effectiveness of the arrays as anti-alias filters can again be seen with less energy wrapping or aliasing occurring on these *f-k* spectra (8d and 8e) at the 15-20 Hz range as compared to the spectrum of the non-arrayed and re-sampled gather. As was seen with the vertical data, the 40 m array again surpasses the 20 m array as an anti-alias filter given that the primary rejection notch of this longer array coincides with the re-sampled spatial nyquist.

2) Post-Stack Array Comparisons

Figures 9, 10 and 11 display the final P-P unmigrated stacks for the non-arrayed data, data arrayed at $L = 40$ and data arrayed at $L = 20$ respectively. For the purpose of clarity, it should be noted that both the non-arrayed and arrayed P-P and P-S stacks have been also spatially re-sampled to the 20 m group interval as was done in the pre-stack array forming. In order to properly visually compare these stacks, a common scalar was applied to all three with the same trace excursion being used for all three. As is evident, these three stacks show little to no difference in the coherency or amplitude of the reflection events present. Figures 12, 13 and 14 display the final P-S unmigrated stacks for the non-arrayed data, data arrayed at $L = 40$ and data arrayed at $L = 20$ respectively. Like the P-P stacks, the same display parameters (common scalar and trace excursion) where applied to the P-S stacks. However, unlike the P-P stacks, the P-S stacks show a significant decrease in the amplitude of the reflection events from the non-arrayed stack to the arrayed stacks. This amplitude decrease is probably best illustrated by observing the amplitudes of the series of three reflectors situated at 1600 ms on the P-S stacks. The greatest decrease is seen between the non-arrayed stack and the stack arrayed at $L = 40$. This decrease also occurs on the stack arrayed at $L = 20$ but not as great as the $L = 40$ stack.

Figure 15 displays the amplitude and phase *f-x* spectra for the P-P non-arrayed stacked data (a and b) as well as the amplitude and phase *f-x* spectra for the P-P arrayed stacks for arrays $L = 40$ (c and d) and $L = 20$ (e and f) for comparison. The amplitude plots of the *f-x* spectra (a, c and e) show good coherency up to 75 Hz and display very subtle differences in the amplitude of these events. The phase plots, which can be a better visual indicator of coherency, show a similar signal band also characterised by a high degree of coherency over the signal band range.

Figure 16 displays the amplitude and phase *f-x* spectra for the P-S non-arrayed stacked data (a and b) as well as the amplitude and phase *f-x* spectra for the P-S arrayed stacks for arrays $L = 40$ (c and d) and $L = 20$ (e and f) for comparison. Both

Contents

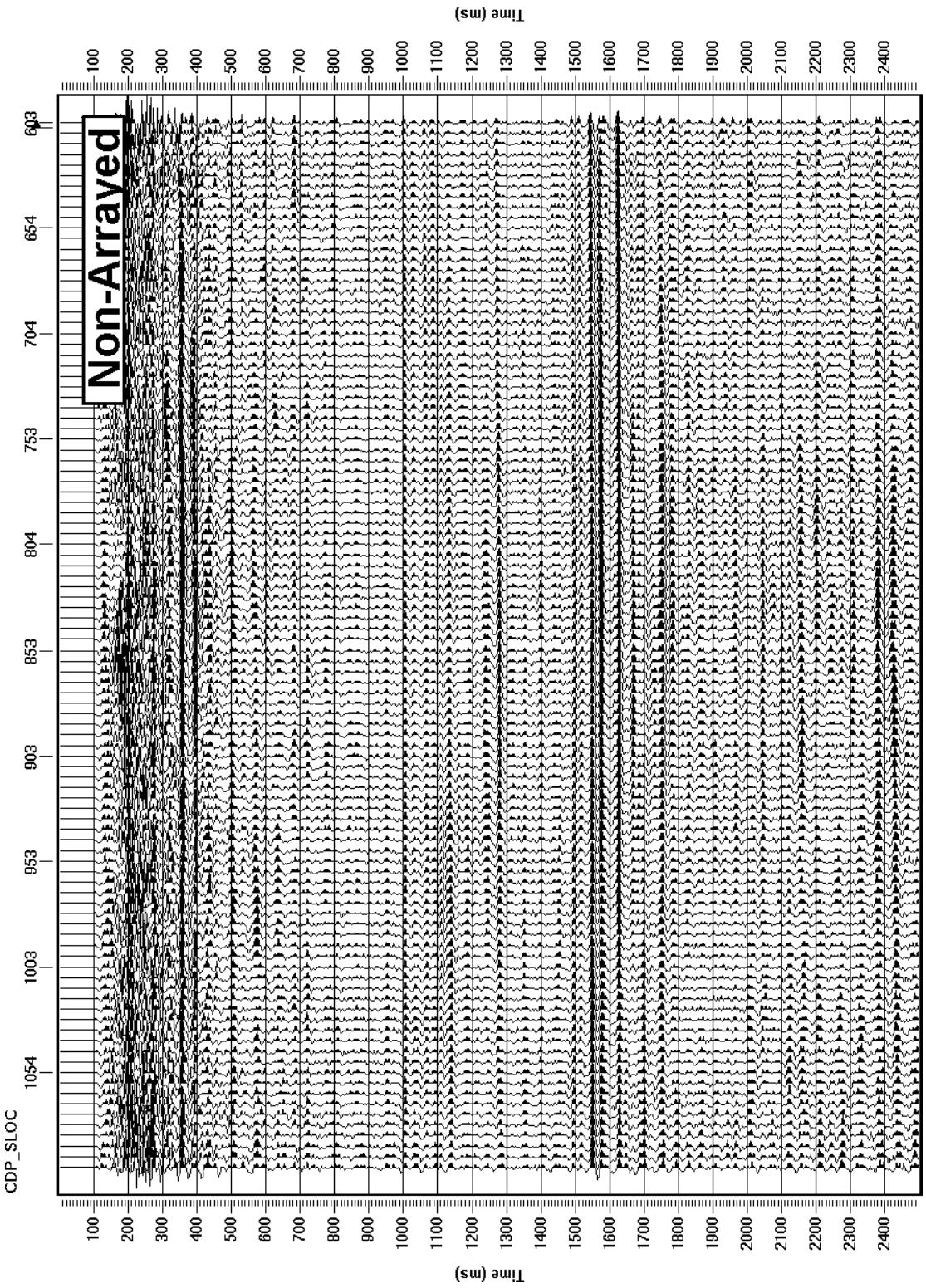

Figure 9. Final P-P unmigrated stack produced from the non-arrayed data. The glauconitic channel is located at approximately 1100 ms.

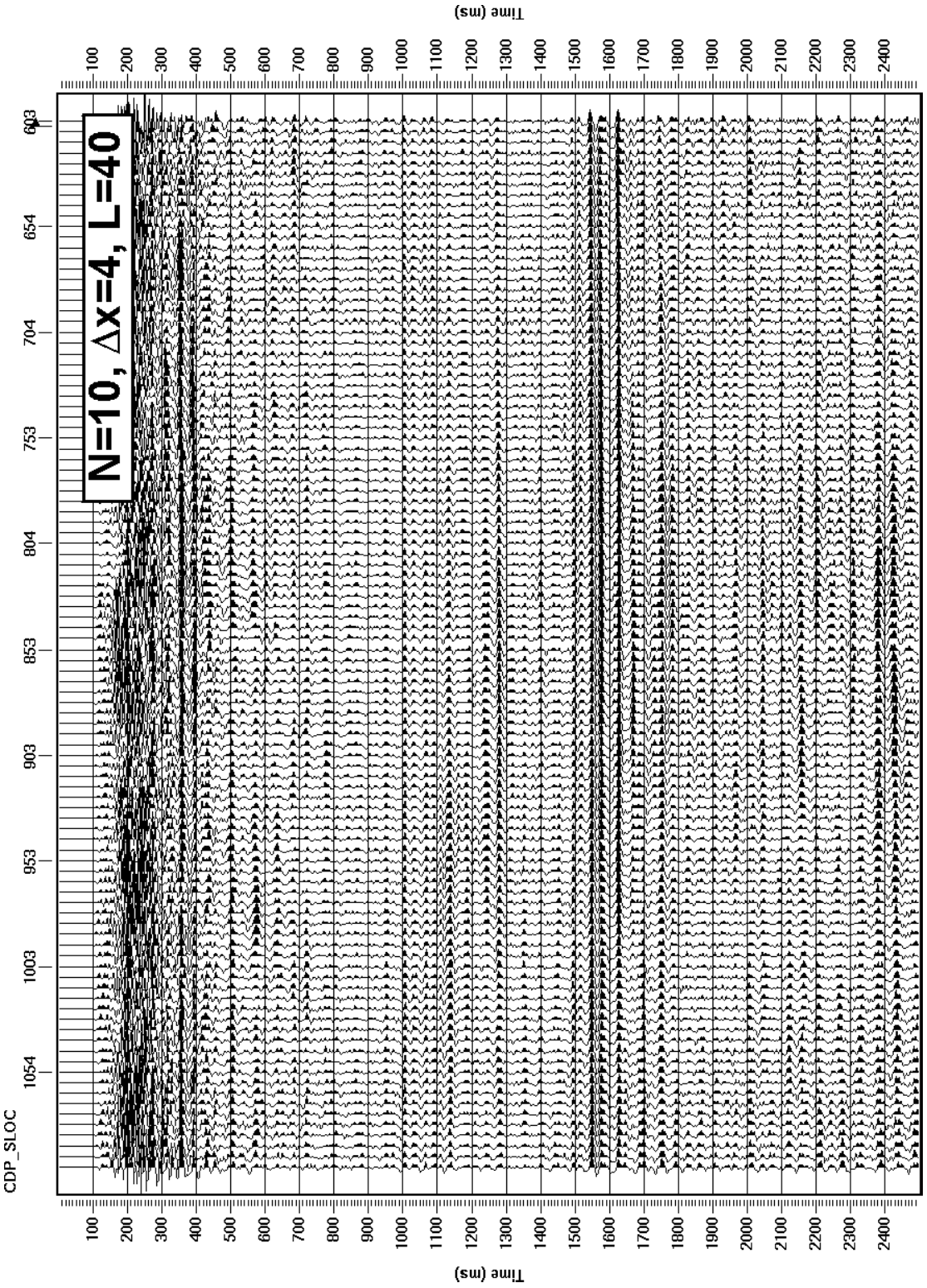

Figure 10. Final P-P unmigrated stack produced from the $L = 40$ arrayed data. The glauconitic channel is located at approximately 1100 ms.

Contents

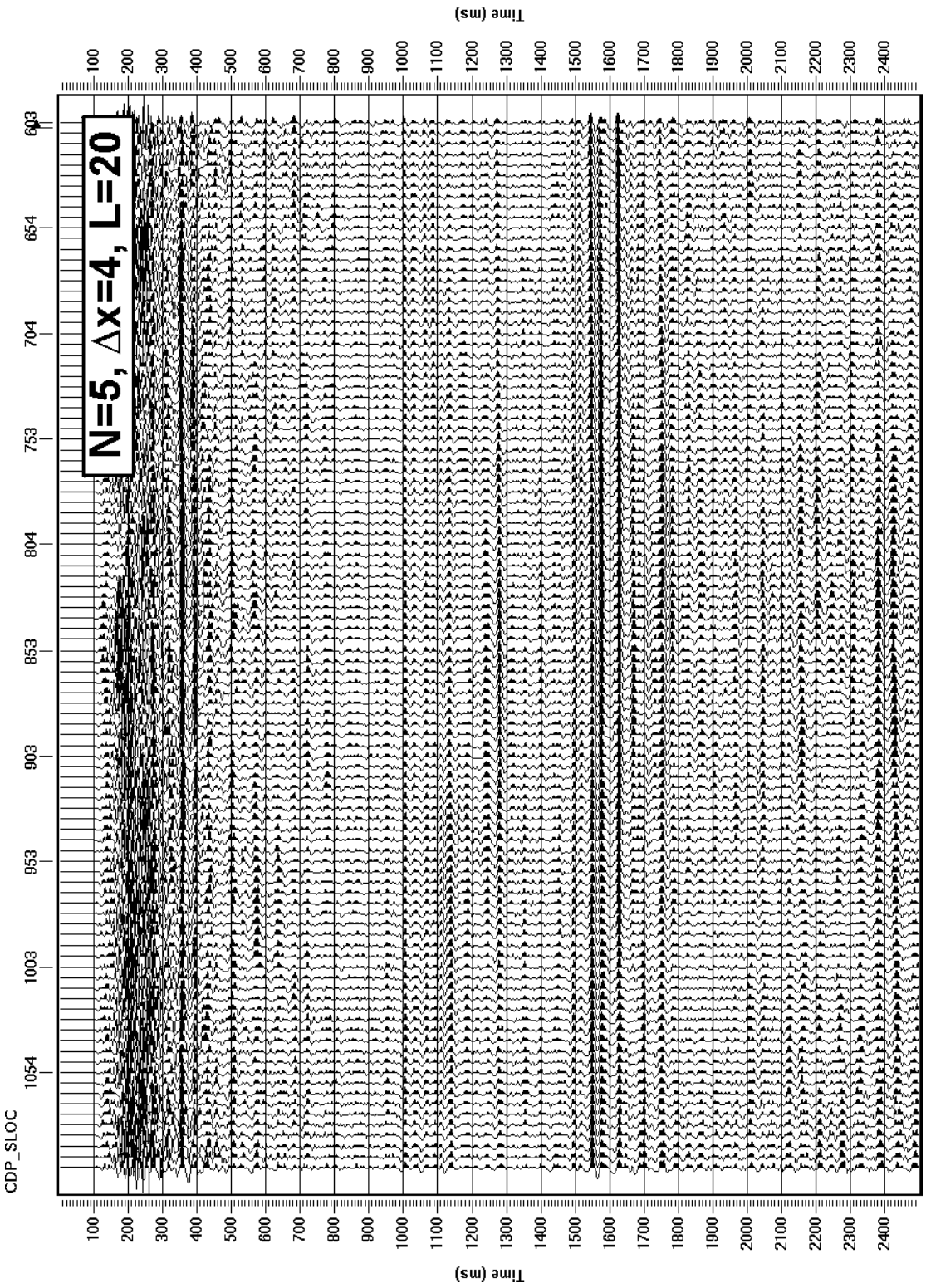

Figure 11. Final P-P unmigrated stack produced from the $L = 20$ arrayed data. The glauconitic channel is located at approximately 1100 ms.

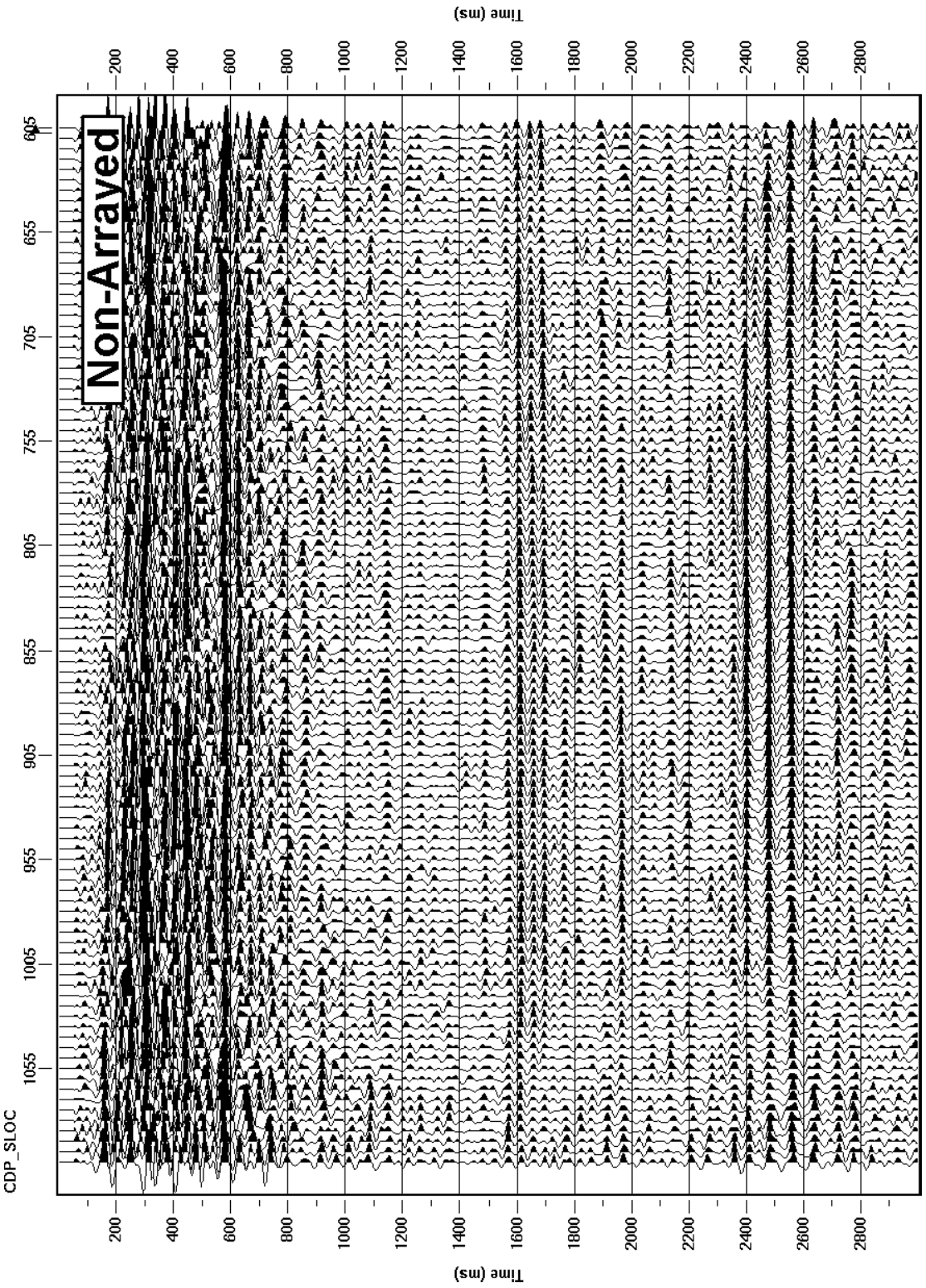

Figure 12. Final P-S unmigrated stack produced from the non-arrayed data. The glauconitic channel is located at approximately 1600 ms.

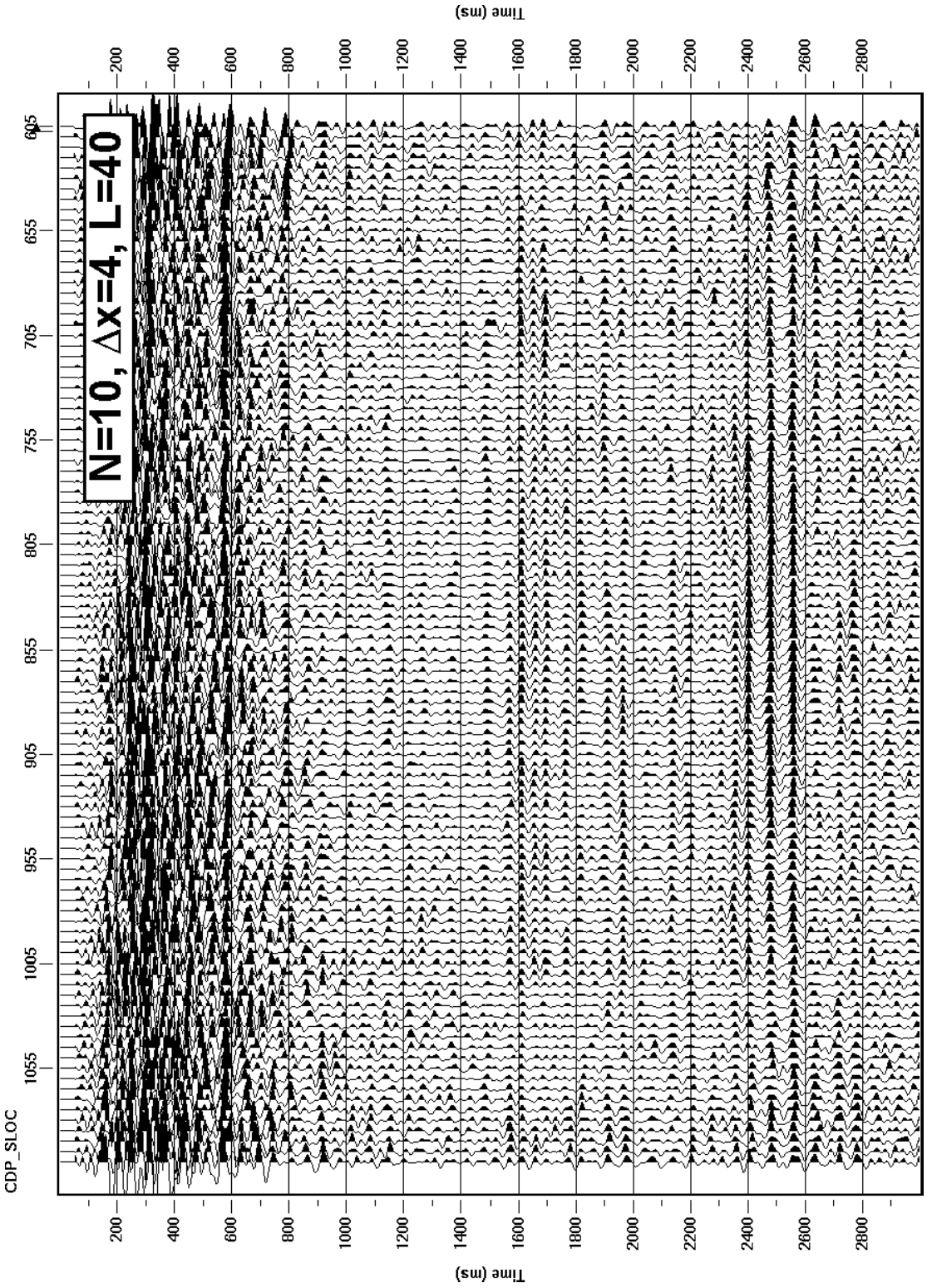

Figure 13. Final P-S unmigrated stack produced from the $L = 40$ arrayed data. The glauconitic channel is located at approximately 1600 ms.

Contents

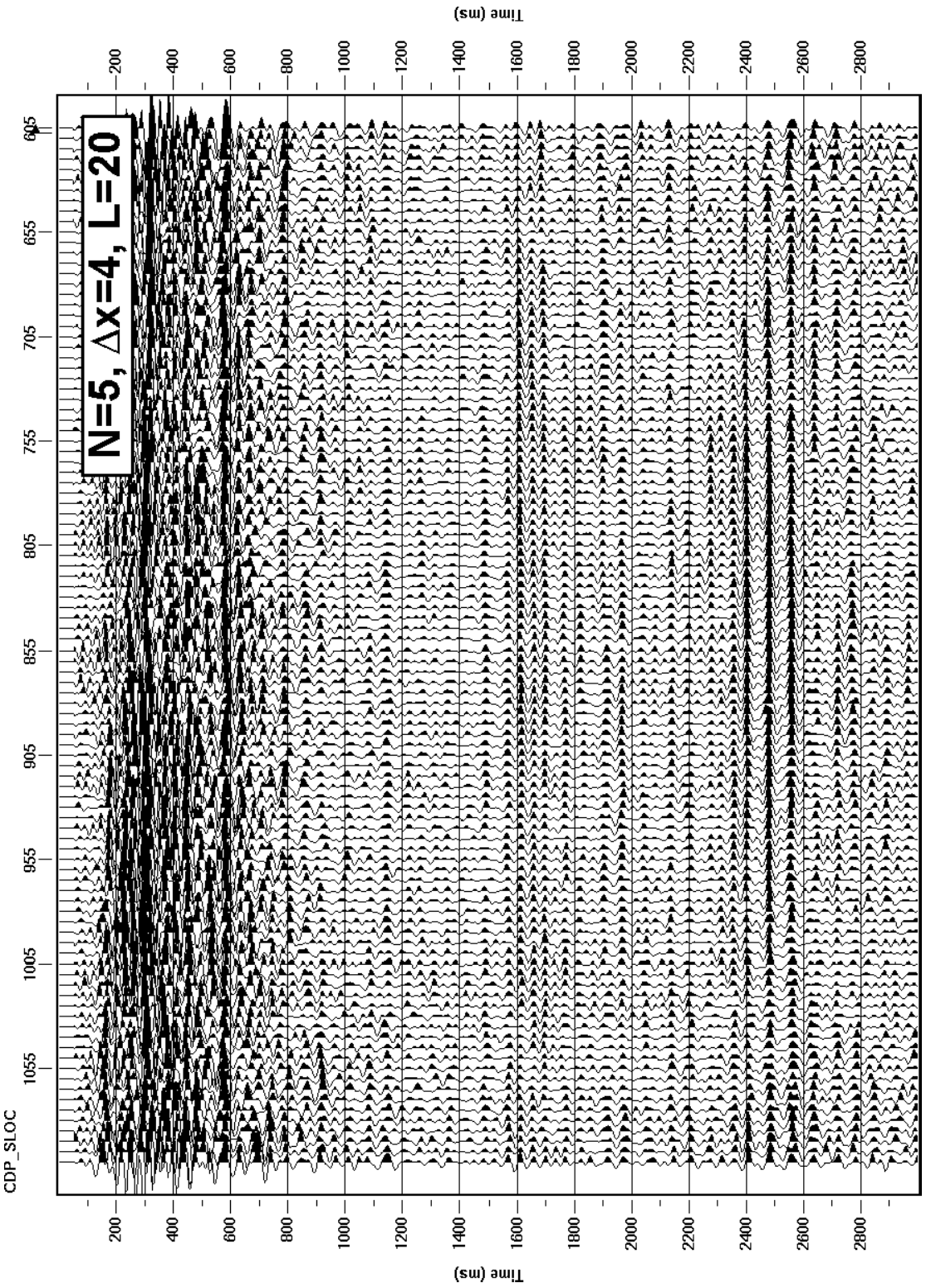

Figure 14. Final P-S unmigrated stack produced from the $L = 20$ arrayed data. The glauconitic channel is located at approximately 1600 ms.

Contents

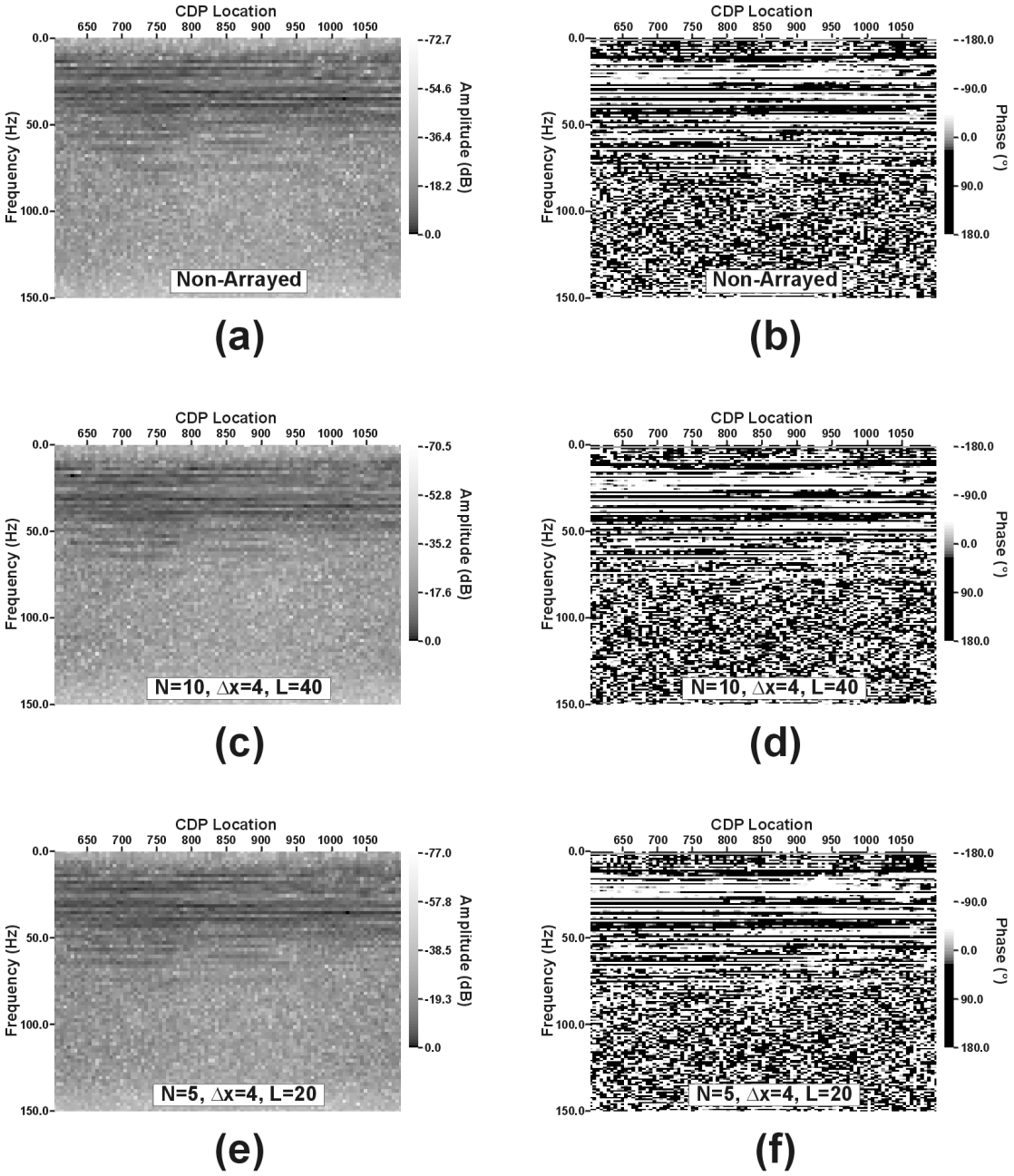

Figure 15. (a) *f-x* amplitude spectrum for the non-arrayed P-P stack and (b) the corresponding *f-x* phase spectrum; (c) *f-x* amplitude spectrum for the $L = 40$ arrayed P-P stack and (d) the corresponding *f-x* phase spectrum; (e) *f-x* amplitude spectrum for the $L = 20$ arrayed P-P stack and (d) the corresponding *f-x* phase spectrum. The analysis window used was 700 – 1200 ms.

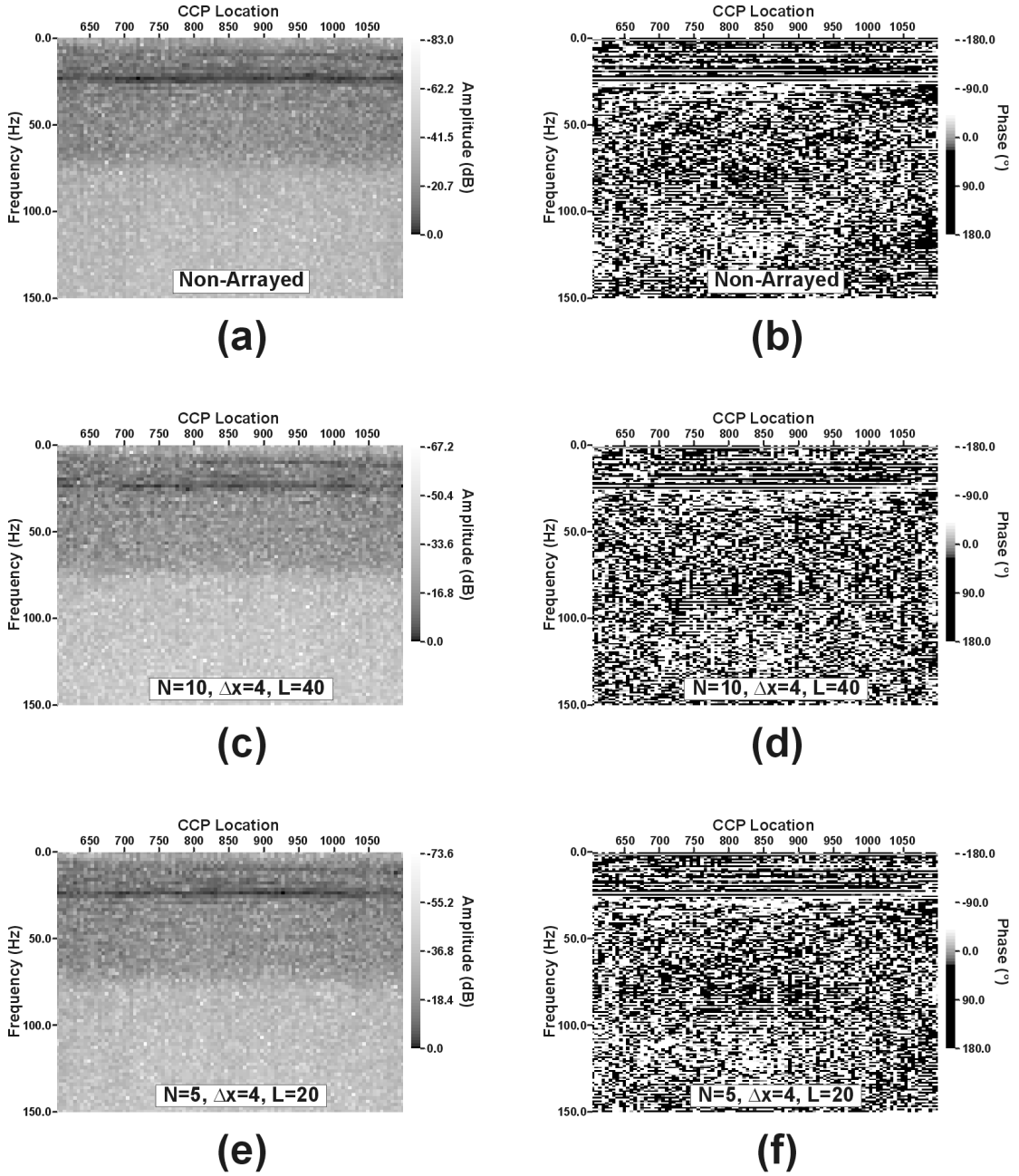

Figure 16. (a) *f-x* amplitude spectrum for the non-arrayed P-S stack and (b) the corresponding *f-x* phase spectrum; (c) *f-x* amplitude spectrum for the $L = 40$ arrayed P-S stack and (d) the corresponding *f-x* phase spectrum; (e) *f-x* amplitude spectrum for the $L = 20$ arrayed P-S stack and (d) the corresponding *f-x* phase spectrum. The analysis window used was 1200 – 1700 ms

amplitude and phase plots of the *f-x* spectra show coherency up to about 35 Hz. However, in the high end of the signal band there is a noticeable difference in amplitude between the non-arrayed and arrayed data. The non-arrayed data shows greater coherency above 25 Hz than either array, with the $L = 40$ array having the worst high-frequency amplitude energy. This observation would seem to support the amplitude differences seen in the *t-x* displays of the P-S stacks.

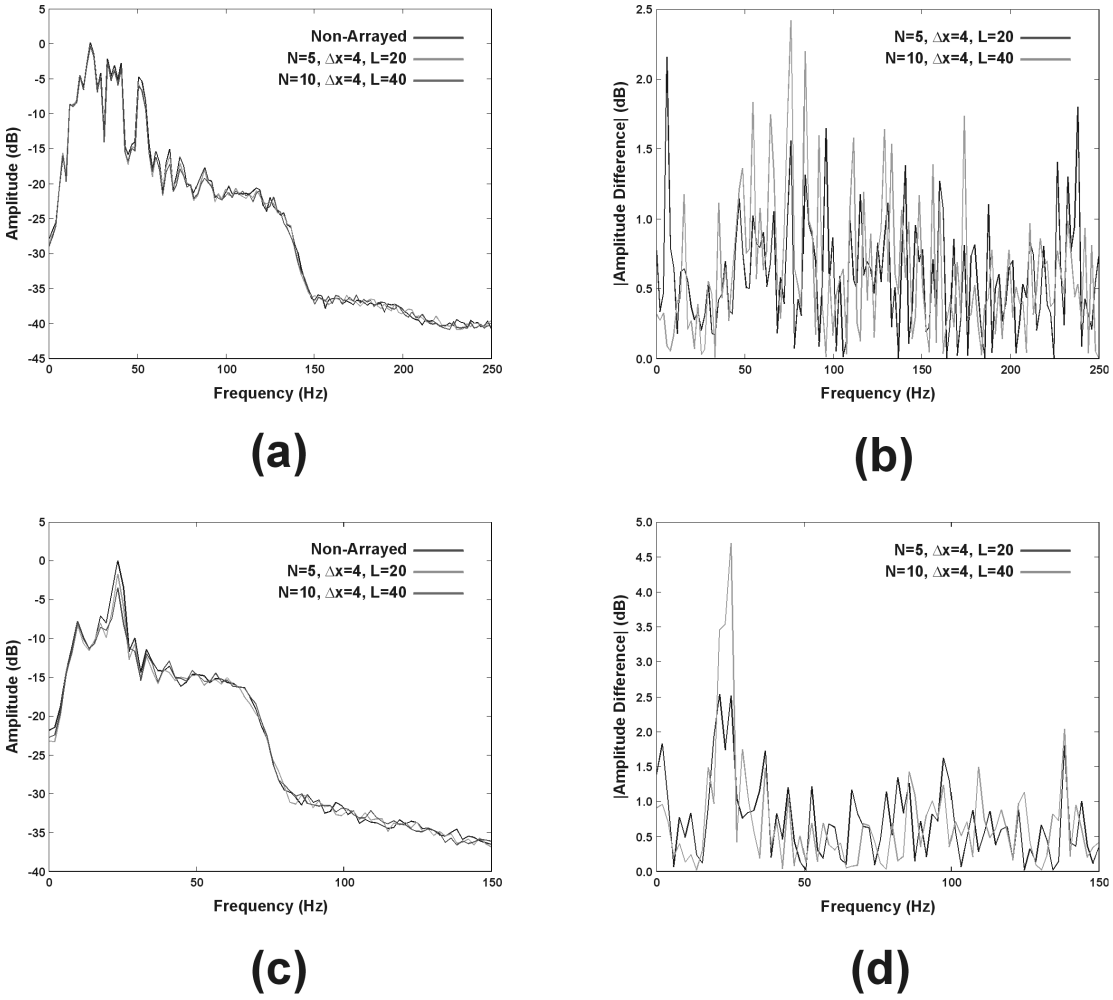

Figure 17. (a) average amplitude spectra for the non-arrayed and arrayed P-P stacks and (b) the absolute value of the difference between spectra for the P-P non-arrayed and arrayed stacks; (c) average amplitude spectra for the non-arrayed and arrayed P-S stacks and (b) the absolute value of the difference between spectra for the P-S non-arrayed and arrayed stacks. The analysis windows used were 700 – 1200 ms and 1200- 1700 ms for P-P and P-S respectively.

Figure 17 displays the average amplitude spectra for the non-arrayed and arrayed stacks as well as the absolute value of the difference between spectra for the non-arrayed and arrayed stacks for both P-P (a and b) and P-S (c and d). The spectral average method did not show any significant differences between the non-arrayed and arrayed P-P stacks. The P-S stacks data showed a noticeable decrease in average signal strength at about 25 Hz with increasing array size. The $L = 20$ array showed a

2.5 dB signal drop at 25 Hz from the non-arrayed spectrum and the $L = 40$ array showing the greatest decrease with a 4.5 dB drop, also at 25 Hz (see Figure 17d).

Figure 18 displays the semblance curves for the non-arrayed and $L = 40$ arrayed P-P and P-S stacked data (a and b respectively), non-arrayed and $L = 20$ arrayed P-P and P-S stacked data (c and d respectively) and the absolute value of the semblance difference between the non-arrayed and arrays $L = 20$ and $L = 40$ of the P-P and P-S stacked data (e and f respectively). The semblance curve for a completely random spectrum has been overlaid on (a), (b), (c) and (d) for comparison purposes. The only noticeable difference in the P-P semblance plots (a, c and e) was outside the signal band in the range of 70 to 120 Hz. This can probably be attributed to a processing artefact due to the application of TV spectral whitening. There appears to be significant differences in the P-S semblance plots (b, d and f), both at the low end of the signal band (0-10 Hz) and the middle to high end (30-50 Hz). Consistently, the $L = 40$ array showed a more marked decrease in semblance than the $L = 20$ array, and both showed less semblance than the non-arrayed data in these two frequency bands.

CONCLUSIONS

By using the Blackfoot high-resolution 3-C data we successfully tested the effectiveness of two differing approaches to array design. In the pre-stack analysis, both arrays were found to be effective in suppressing coherent noise on both the vertical and P-S source gathers. In addition to their noise suppression abilities, both arrays performed reasonably well as anti-alias filters. For the post-stack analysis, three final unmigrated stack sections were produced for both P-P and P-S data, using non-arrayed, group-interval length arrayed ($L = \Delta G$), and twice group-interval arrayed data ($L = 2\Delta G$). For both the P-P data and the P-S data neither of the two tested array designs improved the quality of the final seismic image over the image obtained from non-arrayed data. For P-P data there was no discernible difference between the three final sections, and for the P-S data there was a noticeable deterioration in image quality with increasing array length. Thus we conclude that for the Blackfoot area, given the source configuration used, geophone arrays are unnecessary for P-P data acquisition and are certainly detrimental to P-S data quality.

We believe, although not proven here, that the deterioration witnessed in the arrayed P-S stacks could probably be related to either: (a) the normal moveout or NMO of the converted wave reflections, (b) inter-array converted wave static differences or a combination of both.

Since P-wave and S-wave velocities differ roughly by a factor of 2, a converted wave reflection (P down – S up) will exhibit a steeper moveout curve than its P-P counterpart from the same interface (i.e. slower velocity). Thus, in *t-x* space, the limbs of the converted wave reflection hyperbola at longer offsets may become parallel or sub-parallel to the linear moveout of the coherent noise. Upon transformation to the *f-k* domain, this converted wave reflection energy will map to the higher wavenumbers and possess a finite apparent velocity similar in magnitude to that of the coherent noise. Since the reject band of most array responses tends to be situated at the these higher wavenumbers, the array will substantially attenuate this

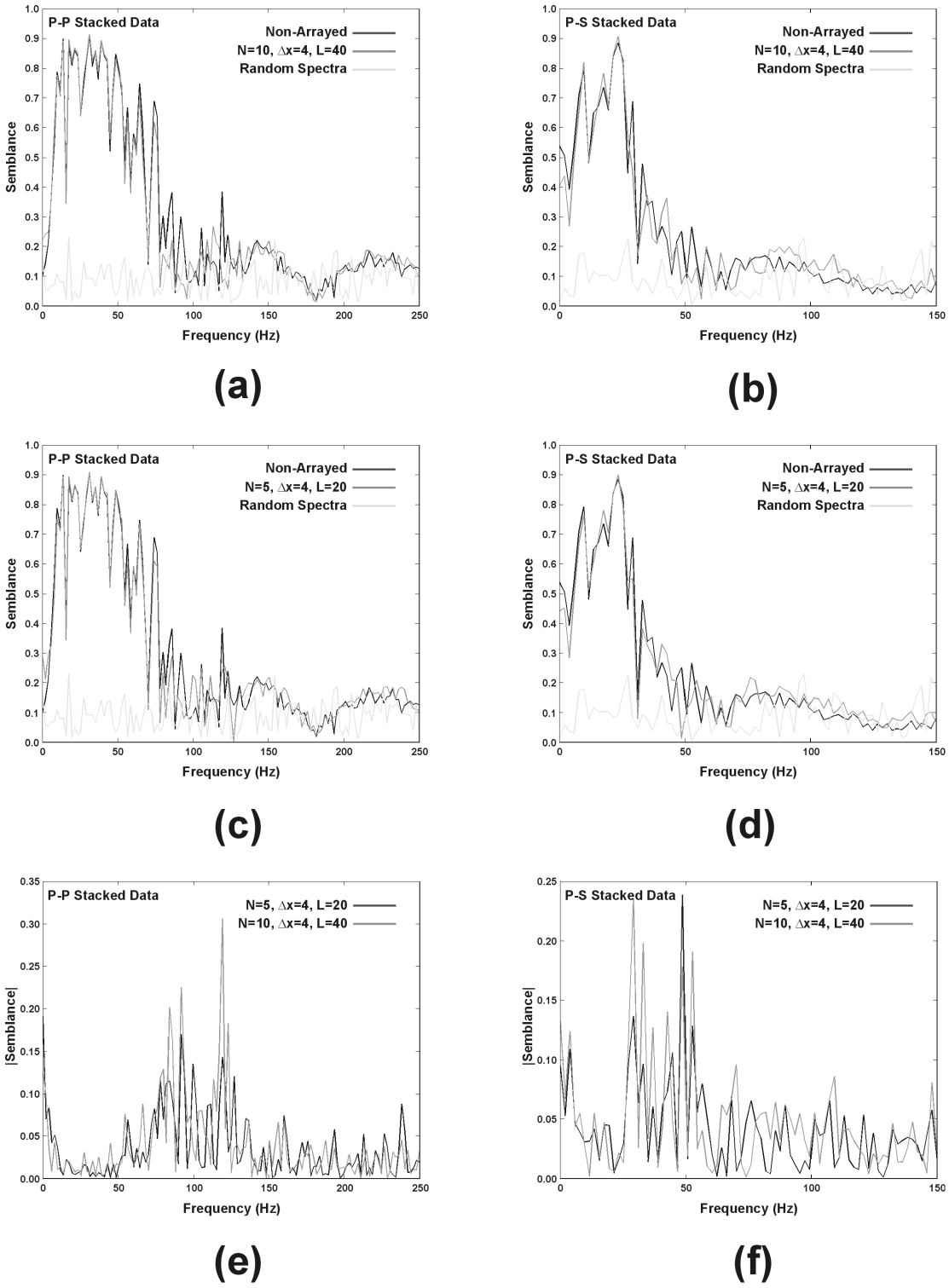

Figure 18. (a) semblance curves for the non-arrayed and $L = 40$ arrayed P-P stacked data and (b) corresponding curves for the P-S stacked data; (c) semblance curves for the non-arrayed and $L = 20$ arrayed P-P stacked data and (d) corresponding curves for the P-S stacked data; (e) semblance difference curves between the non-arrayed and arrays $L = 20$ and $L = 40$ of the P-P stacked data and (f) corresponding curves for the P-S stacked data. The analysis windows used were 700 – 1200 ms and 1200- 1700 ms for P-P and P-S respectively.

Contents

portion of the converted wave reflection energy. However, a very preliminary investigation (not ready at time of press) into the interaction of the normal moveout of the converted wave reflections with the arraying process has suggested that it may not be a large factor in the deterioration in the quality of the final arrayed P-S images.

Another possible explanation for the noticeable deterioration observed in the arrayed P-S stacks may be due to significant converted wave static differences among the individual elements of the array itself. One could imagine if such local static differences did exist, then arraying could lead to a degradation of reflector energy at the summed output of the array. In essence, depending on their magnitude, these static shifts could introduce considerable phase differences in the converted wave reflected energy among each of the array elements. Thus array summing these phase-differenced traces could be detrimental to the converted wave reflection energy which is the primary objective of the multicomponent recording.

FUTURE WORK

The Blackfoot high-resolution 3-C data offer many exciting research possibilities. As demonstrated in this paper, this data set may be particular useful in trying to solve some of the more practical problems dealing with the acquisition of multicomponent seismic data. One pressing issue, as raised in the conclusions, would be to ascertain the reason or reasons as to why there is an observed degradation in the quality of the final P-S stacks produced from the arraying. Another particular direction which would be worthwhile pursuing is the simulation of the effects of random misorientation within a 3-C geophone array on the final P-P and P-S stacked images. Also, given the 2 m spacing of the high-resolution data, many other array configurations could also be tested. For future high-resolution 3-C data sets to test array design, it would be very useful to deploy various sources. Field recordings of a surface seismic source such as Vibroseis would most certainly be dominated by strong ground roll and air blast and the value of 3-C arrays could be more fully evaluated under these conditions.

ACKNOWLEDGEMENTS

We would like to thank William Goodway and David Cooper of PanCanadian Petroleum Ltd. and John Boyd and Doug Eaton of Boyd PetroSearch for all their assistance in successfully acquiring this unique 3-C survey. We also thank Mark Harrison of Matrix GeoServices Ltd. who kindly provided us with the ProMAX ™ processing archive. Finally, we thank all sponsors of the CREWES Project for their continued technical and financial support.

REFERENCES

Hoffe, B. H., Stewart, R. R., Bland, H. C., Gallant, E. V. and Bertram, M. B. 1998. The Blackfoot high-resolution 3-C seismic survey: design and initial results: Expanded abstract, Soc, Expl. Geophys. 68th Annual Meeting, New Orleans, LA

Margrave, G. F., 1995. Estimates of the signal bandwidth of the Blackfoot broad-band data: CREWES Research Report, **7**, Chapter 39.

Newman, P. and Mahoney, J. T., 1973. Patterns with a pinch of salt: Geophysical Prospecting, **21**, 197-219.

Ongkiehong, L. and Askin, H. J., 1988. Towards the universal seismic acquisition technique: First Break, **6,** no. 2, 46-63.

Ongkiehong, L. and Huizer, W., 1987. Dynamic range of the seismic system: First Break, **5,** no. 12, 435-439.

Stone, D. G., 1994. Designing surveys in two and three dimensions: Soc. Expl. Geophys.